Available online at www.sciencedirect.com

ScienceDirect

Advances in Space Research 63 (2019) 1554–1565

ADVANCES IN SPACE RESEARCH (a COSPAR publication)

www.elsevier.com/locate/asr

# A novel predictive algorithm for double difference observations of obstructed BeiDou geostationary earth orbit (GEO) satellites

Yuan Du [a], Guanwen Huang [a,*], Qin Zhang [a,*], Rui Tu [b], Junqiang Han [a], Xingyuan Yan [a], Xiaolei Wang [a]

[a] College of Geology Engineering and Geomatic, Chang'an University, 126 Yanta Road, Xi'an 710054, China
[b] National Time Service Center, Chinese Academy of Sciences, Shu Yuan Road, 710600 Xi'An, China

Received 5 July 2018; received in revised form 8 November 2018; accepted 12 November 2018
Available online 20 November 2018

**Abstract**

Transmission link disturbances and device failure cause global navigation satellite system (GNSS) receivers to miss observations, leading to poor accuracy in real-time kinematic (RTK) positioning. Previously described solutions for this problem are influenced by the length of the prediction period, or are unable to account for changes in receiver state because they use information from previous epochs to make predictions. We propose an algorithm for predicting double difference (DD) observations of obstructed BeiDou navigation system (BDS) GEO satellites. Our approach adopts the first-degree polynomial function for predicting missing observations. We introduce a Douglas-Peucker algorithm to judge the state of the rover receiver to reduce the impact of predictive biases. Static and kinematic experiments were carried out on BDS observations to evaluate the proposed algorithm. The results of our navigation experiment demonstrate that RTK positioning accuracy is improved from meter to decimeter level with fixed ambiguity (horizontal $< 2$ cm, vertical $< 18$ cm). Horizontal accuracy is improved by over 50%, and the vertical accuracies of the results of the static and kinematic experiments are increased by 47% and 27% respectively, compared with the results produced by the classical approach. Though as the baseline becomes longer, the accuracy is weakened, our predictive algorithm is an improvement over existing approaches to overcome the issue of missing data.


*Keywords:* BDS GEO; Double difference observation prediction; RTK; Douglas-Peucker

## 1. Introduction

Since December 27, 2012, the Chinese BeiDou-2 regional navigation system has provided regional positioning, navigation, and timing (PNT) services across the Asia-Pacific region. The performance of BDS RTK has been assessed in many studies. Static relative positioning of the baseline reaches millimeter-level precision (He et al., 2013; Teunissen et al., 2014). These levels of precision are close to the levels achieved by Global Positioning System (GPS) (Shi et al., 2013; Yang et al., 2011; Jin, 2016; Montenbruck et al., 2015). At present, global navigation satellite system (GNSS) real–time kinematic (RTK) positioning technology can reach centimeter or even millimeter-level precision by successfully fixing carrier phase ambiguities in a good environment (Teunissen et al., 1997). In order to eliminate related systematic error, the classical synchronous RTK technique requires the reference station and rover station both to receive their signals from the same satellites simultaneously. However, owing to transmission link disturbances, urban canyon and device failure, GNSS receivers often lose information from obser-

* Corresponding authors.
*E-mail addresses:* huang830928@163.com (G. Huang), zhangqinle@263.net.cn (Q. Zhang), turui@ntsc.ac.cn (R. Tu).

https://doi.org/10.1016/j.asr.2018.11.009
0273-1177/

vations, causing poor accuracy in RTK positioning or unavailability of positioning results.

To overcome the problem of missing observations in GNSS, the classical solution involves the prediction of current coordinates from past information or prediction of reference station observations. In terms of RTK prediction methods, Lawrence proposed reference carrier phase prediction (RCPP) technology for kinematic GPS, which could provide 10 s reference phase predictions with an accuracy of 10 cm based on data from about 7 s in the past. As the predicting (or latency) time increased, the results gradually deteriorated (Lawrence, 1999). In the case of a short-term loss of observations, the sampling rate of observations from the reference receiver may differ from that of the rover receiver. Usually, the high-sampling receiver is diluted to yield the same data intervals as the low-sampling receiver, and some observations are discarded. Similarly, when only one receiver receives a signal from a satellite that is not observed by the other receiver, observations from this satellite are discarded. Wang proposed a processing strategy to address the different data sampling rates of GPS rover and reference receivers, but it was mainly used for post-processing (Wang et al., 2011). For real-time positioning applications, Zhang developed an asynchronous RTK (ARTK) method using asynchronous double difference (DD) observations from two receivers. The accuracy of ARTK positioning, including the influence of ephemeris error and atmospheric delays, was studied in detail. Broadcast ephemeris was used to eliminate the impact of satellite clock error, and an acceptable positioning accuracy for common users was consequently obtained (Zhang et al., 2015). In short, the previous methods mainly focused on the problem of the reference receiver missing the carrier phase. However, observation loss by the rover receiver is a more serious issue that is easily caused by a complex environment. Previously described methods do not address this problem and are unable to predict lost rover observations.

The Chinese BDS navigation system is different from other GNSSs because of its special constellation, which consists of satellites in geostationary earth orbit (GEO), inclined geosynchronous earth orbit (IGSO), and medium earth orbit (MEO). Considering the geostationary character of BDS GEO satellites (the fact that the relative space positions of different GEO satellites remain approximately constant), the observations from different GEO satellites exhibit strong correlation, so obstructed GEO satellite observations can be predicted using observations from visible GEO satellites. Based on this principle, our study proposes a novel algorithm for predicting DD observations of obstructed BDS GEO satellites. To determine the best predictors, the minimum mean squared error (MMSE) criterion is often used. The best linear unbiased prediction (BLUP) is known as the predictor with the best statistical properties (Teunissen, 2013). Instead of the Kalman filter, which works with known state-vector means, the BLUP method relaxes the model and assumes these means to be unknown. Because dynamic modeling of DD observations is difficult to understand, the Kalman filter without dynamic modeling is equivalent to the best linear predictor with MMSE criterion. Under MMSE criterion the first-degree polynomial function is used to predict the lost observations. Further, a Douglas-Peucker (D-P) algorithm (Douglas and Peucker, 2011) is introduced to judge the state of the rover receiver, thus reducing the impact of predictive biases. The proposed algorithm is not affected by the predicting time when the state of the receiver is maintained and it maximizes the utilization of observations from other satellites, unlike the direct prediction of coordinates employed by conventional methods.

We validated our proposed algorithm by performing static and kinematic experiments. Our predictive algorithm is an improvement over existing approaches to overcome the issue of missing data in satellite observations.

## 2. Materials and methods

### 2.1. The DD model

The DD model is often applied in RTK positioning technology. The undifferenced carrier-phase observation equation relating the BDS satellites $s$ and the receiver $r$ is given as (Xu and Xu, 2016):

$$\lambda\phi_r^s = R_r^s + c(\delta t_r - \delta t^s) + \lambda N_r^s + \mathrm{T} - \mathrm{I} + \delta_{tide} + \delta_{rel} + \varepsilon, \tag{1}$$

where $\lambda$ is the signal wavelength, the subscript $r$ indicates the receiver $r$, superscript $s$ indicates the satellite number, $R$ is the geometry range between the satellite and the receiver, c is the velocity of light, $\delta t_r$ and $\delta t^s$ are clock errors of the receiver and the satellite, $N$ is the carrier phase ambiguity in cycles, and $\mathrm{T}, \mathrm{I}, \delta_{\mathrm{tide}}, \mathrm{and}\delta_{\mathrm{rel}}$ are errors caused by the troposphere, ionosphere, tide, and relativistic effect, respectively. $\varepsilon$ is random observation error.

A simplified DD observation model that eliminates correlation error and ignores the impact of observation noise is given as (Comstock, 2006; Tu et al., 2017a, 2017b):

$$\lambda\Delta\nabla\phi_r^s = \left(e^j - e^k\right)\Delta X + \lambda\Delta\nabla N_{b,r}^{j,k}, \tag{2}$$

where $\Delta\nabla$ indicates DD and $\Delta$X is the coordinate difference between reference and rover satellites and includes three parameters – $\Delta x, \Delta y, \Delta z$. The superscripts $j$ and $k$ indicate satellite numbers, the subscripts $b$ and $r$ indicate the reference receiver $b$ and the rover receiver $r$ respectively, and $e^j$ represents the coefficient related to satellite j.

In order to express the coordinate corrections in a topocentric coordinate system, $X = [E\ N\ U]^T$ is obtained by multiplying the coefficient matrix $R$ and is given as (Leick, 2004):

$$X = R \cdot \Delta X = \begin{Bmatrix} -\sin\varphi\cdot\sin\eta & \cos\eta & \cos\varphi\cdot\sin\eta \\ -\sin\varphi\cdot\cos\eta & -\sin\eta & \cos\varphi\cdot\cos\eta \\ \cos\varphi & 0 & \sin\varphi \end{Bmatrix} \cdot \begin{Bmatrix} \Delta x \\ \Delta y \\ \Delta z \end{Bmatrix}, \tag{3}$$

where $\varphi$ and $\eta$ are the nominal latitude and longitude of the station.

GNSS RTK technology at its present level of advancement could easily achieve centimeter-level accuracy in a good environment. However, transmission link blocks and receiver failure often lead to the partial loss of GNSS receiver observations, which results in poor RTK positioning results, or unavailable results. We tried to find a method to resolve this problem using the relationship between the obstructed satellite and other satellites in terms of spatial distribution to predict the lost DD observations for positioning and calculation.

### 2.2. Spatial correlation between BDS GEO satellites

Since December 27, 2012, the BeiDou-2 regional navigation system has provided PNT services across the Asia-Pacific region. By 2020, the BeiDou-3, with 35 satellites in orbit, will provide PNT services worldwide. The system includes three types of orbit satellites. All satellites of a particular type exhibit the same orbital space distribution. The five GEO satellites are fixed at 58.75°, 80°, 110.5°, 140°, and 160° east longitudes respectively, and their relative positions are stable. First, C10, which belongs to the BDS IGSO satellites, is chosen as a reference satellite. Figs. 1 and 2 show the correlation between L1 and L2 DD observations between the C01 satellite and other GEO satellites. Fig. 1 shows the sequence of DD observations for C01 and C04, and Fig. 2 shows the correlation statistic between DD observations from C01 and observations from the other GEO satellites. We found a high correlation between the DD observations.

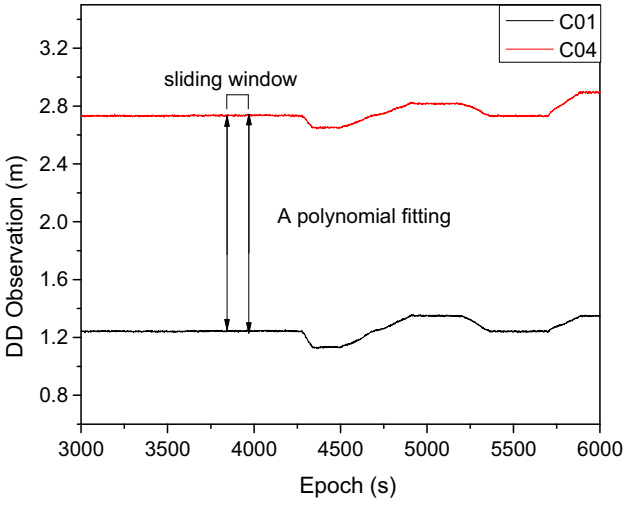


Fig. 1. C01-C04 DD observations. The baseline is 30 m. The rover receiver is in a static state before approximately 4500 epochs and then in a simulated slow-deformation state.

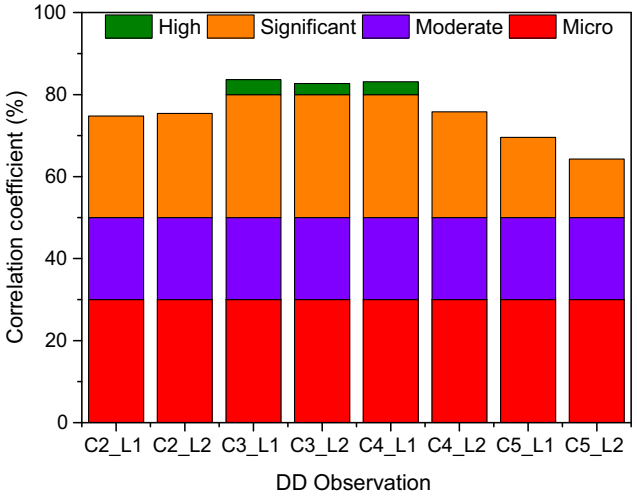


Fig. 2. Correlation between C01 and other GEO satellites in terms of DD observations.

### 2.3. DD observation prediction

For reference satellite $j$, all observations can be obtained using the following equation (correlation error (atmospheric delays) can be neglected in the short-baseline case ($\leq$10 km) (seen from Takasu and Yasuda, 2010)):

$$\begin{bmatrix} \Delta\nabla\phi_{b,r}^{j,i} \\ \cdots \\ \Delta\nabla\phi_{b,r}^{j,k} \\ \cdots \\ \Delta\nabla\phi_{b,r}^{j,l} \end{bmatrix} = \begin{bmatrix} \lambda^{-1}(e^j - e^i) & 1 & 0 & 0 & 0 & 0 \\ \cdots & 0 & \cdots & 0 & 0 & 0 \\ \lambda^{-1}(e^j - e^k) & 0 & 0 & 1 & 0 & 0 \\ \cdots & 0 & 0 & 0 & \cdots & 0 \\ \lambda^{-1}(e^j - e^l) & 0 & 0 & 0 & 0 & 0 \end{bmatrix} \begin{bmatrix} \Delta x \\ \Delta y \\ \Delta z \\ \Delta\nabla N_{b,r}^{j,i} \\ \cdots \\ \Delta\nabla N_{b,r}^{j,k} \\ \cdots \\ \Delta\nabla N_{b,r}^{j,l} \end{bmatrix}. \tag{4}$$

If a problem with satellite $k$ at the reference or rover receivers is caused by receiver failure, transmission link blockage, or obstruction, the integer ambiguity parameter in formula (4) does not change, so the change in coordinates is related only to the DD observations. First of all, the RTK positioning algorithm in this paper is a fixed calculation of single-epoch ambiguity. Under this condition, we can ignore the problem of cycle slip detection as we do in the single-epoch ambiguity method. Secondly, the premise of the prediction is that the current epoch is missing data, so there is no fact that a cycle slip occurs. It is assumed that the ambiguity has not changed, just to better predict the observations, which does not affect the fixed RTK solution with single-epoch ambiguity. Therefore, to the DD observation for GEO satellite $i$, the difference between satellite $i$ and satellite $k$ is added in order to accurately estimate the DD observation for GEO satellite $k$, which is similar to satellites 1 and 4 (Fig. 1). Its formula is given as:

$$\Delta\nabla\phi_{b,r}^{j,k} = \Delta\nabla\phi_{b,r}^{j,i} + X_i \tag{5}$$

where $X_i$ is the difference between the DD observations. It can be seen that $\Delta\nabla\phi_{b,r}^{j,k}$ consists of $\Delta\nabla\phi_{b,r}^{j,i}$ and $X_i$. While the vehicle turning its direction, the $\Delta\nabla\phi_{b,r}^{j,i}$ changes with it. Therefore, $\Delta\nabla\phi_{b,r}^{j,k}$ may contain some information about the direction of the vehicle.

The difference between these two DD observations is slowly time varying and can be modeled in the time domain. The first-degree polynomial function is a straightforward option for predicting the difference and is given as:

$$X_i = a_0 + a_1 t_i + \varepsilon_i \quad (0 \leqslant i \leqslant n), \tag{6}$$

where $t_i$ is the epoch time, $a_0$, and $a_1$ are the model parameters, $\varepsilon_i$ is the model error, and n is the sliding window size.

The first-order polynomial is simple with a high short-term fitting prediction accuracy, so it is widely used in GNSS real-time navigation and positioning (Huang and Zhang, 2012). In Table 1, the prediction root mean square (RMS) residuals of static DD observations are presented, where M represents the polynomial order and 1 min indicates the duration of time for which the observation is made. L1 and L2 are observation frequencies. Table 2 shows the prediction residuals of kinematic DD observations. For a total of 2.5 h of data, the sampling rate is 1 Hz and the sliding window size is adaptively adjusted according to the state of the receiver (as shown in Section 2.4) in the Tables 1 and 2.

It can be seen from Table 1 that for short-term interruptions, the prediction accuracy of the first-order polynomial is higher than that of the second-order polynomial. As the interruption time increases, the result of the first-order polynomial does not deteriorate, but the dynamic one does as shown in Table 2. In this study, we assume that the short-term interruption is 1 min. In order to verify the efficiency of the proposed algorithm, traditional coordinate sequence information is used in the coordinate prediction algorithm (which also uses the first-order polynomial). Under this condition, $X_i$ is the coordinates.

### 2.4. Douglas-Peucker algorithm

For static observations, in case of short-term loss, DD observations can be predicted using a polynomial with a fixed sliding window size. The window size of the dynamic observation must be adaptively adjusted according to the state of the receiver. When the receiver state changes, the information in the window before the moment at which the alteration is made must be deleted to improve prediction accuracy. In order to judge the state of the receiver, we introduce a D-P algorithm, as originally proposed by Douglas and Peucker in 1973. The purpose of the D-P algorithm is, to determine a curve using fewer points that is similar to a given curve comprising multiple line segments (also called a polyline in some contexts). The original curve consists of eight points. The point furthest from the line segment consisting of the first and last points as end points is determined as shown in Fig. 3a (1). Point 4 is obviously furthest from the line segment between the first and last points as end points. Points can be discarded without the simplified curve becoming worse than the distance size that is usually user-defined. Because point 4 from the line segment is greater than distance size, point 4 must be kept. The D-P algorithm recursively calls itself with the first point and point 4 and then with point 4 and the last point, which includes the furthest point being marked. When the recursion (as shown in Fig. 3a (2), (3), and (4)) is completed, a new output curve is obtained. The D-P algorithm simplifies linear elements to identify changes in the state of the receiver has been change, as shown in Fig. 3b. The distance between the reference and the rover receivers set at approximately 30 m, before approximately 3275 epochs, the experiment is static and after is kinematic as shown in Fig. 3b. When the receiver state changes, a turning point that should be marked one is produced in the DD observations sequence. It can be seen from Fig. 3b that DD observations are processed using a sliding window. If there is a turning point in the sliding window, inaccuracies arise in the prediction of DD observations when observations before the turning point are used to predict the DD observations after the turning point. To avoid such prediction biases, the following steps are applied:

1. The window size is selected. In this study, we chose a window length of 30 s, considering the large influence of observation noise for small window.
2. The distance from the middle point of the window to the line at both ends of the window is calculated.
3. When the distance is greater than three times the mean square error of DD observations, the receiver state is regarded as changed. At this time, the information in the sliding window before the state change is deleted, and the ambiguity parameter of the satellite is not fixed (Wu et al., 2016).

### 2.5. Real-time predictive strategy for DD observations of GEO satellites

According to the above model algorithm, the process chart for RTK DD observation prediction is shown in

Table 1
The prediction residuals of static DD observations (RMS unit: m).

| | M = 1 | | M = 2 | |
|---|---|---|---|---|
| | L1 | L2 | L1 | L2 |
| 1 min | 0.003 | 0.004 | 0.025 | 0.026 |
| 2 min | 0.004 | 0.004 | 0.083 | 0.093 |
| 5 min | 0.003 | 0.004 | 0.431 | 0.457 |

Table 2
The prediction residuals of kinematic DD observations (RMS unit: m).

| | M = 1 | | M = 2 | |
|---|---|---|---|---|
| | L1 | L2 | L1 | L2 |
| 1 min | 0.005 | 0.007 | 0.033 | 0.042 |
| 2 min | 0.007 | 0.011 | 0.121 | 0.137 |
| 5 min | 0.020 | 0.021 | 0.488 | 1.013 |

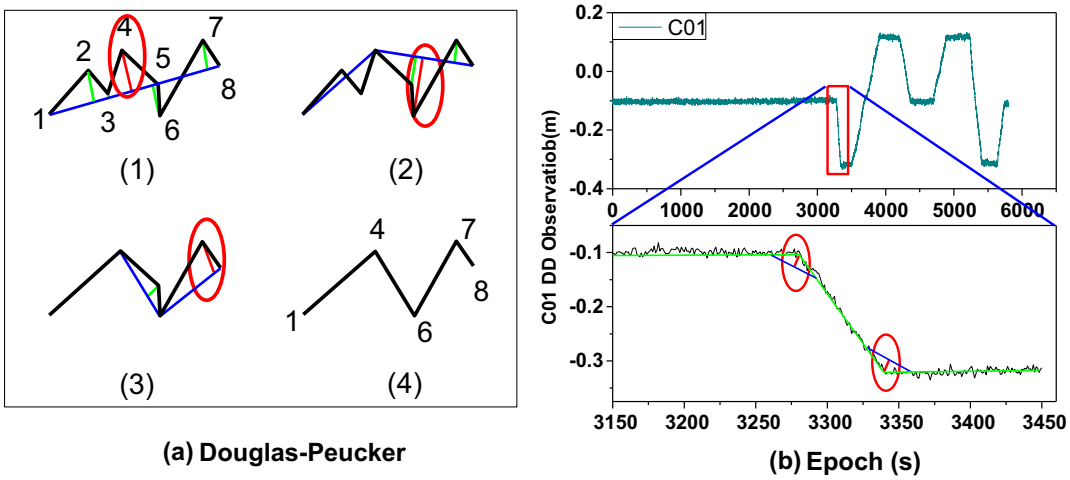


Fig. 3. (a) Simplifying a piecewise linear curve using the D-P algorithm. (b) Application of D-P algorithm in the sequence of DD observations.

Fig. 4. The classical DD model is used to obtain the solution when there is no data loss. If a GEO satellite is missing, the DD observations of this satellite are predicted. If the state of receiver is changed, the partial ambiguity-fixing strategy is adopted. The steps for our real-time DD observation prediction algorithm are given below.

1. Start the program and initialize the structure.
2. Read data.
3. Solve the first epoch using the traditional DD model.
4. Judge whether any satellite loss at the current epoch appears: if there is loss, DD observations are predicted, and state judgment is performed to determine whether the partial ambiguity-fixing strategy should be introduced.
5. Output the solved result.
6. Loop the last epoch.

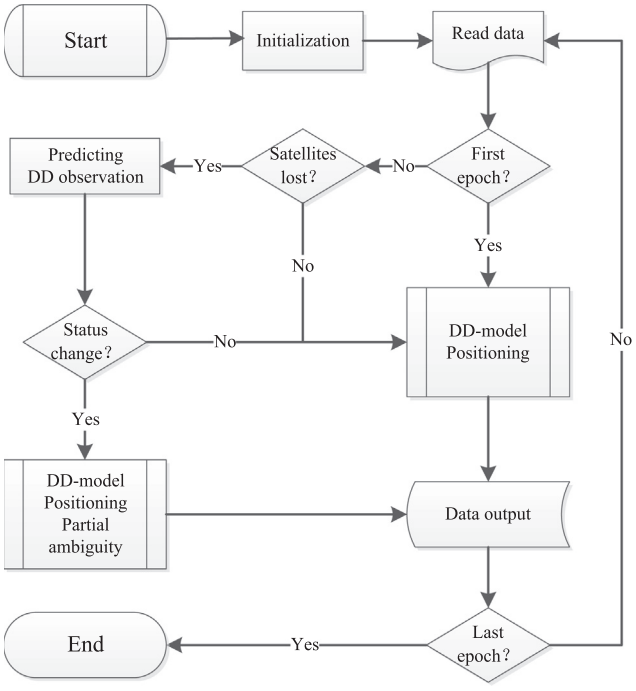


Fig. 4. Flow chart of real-time DD observations predicting.

(Note that: It takes about 0.07 s to process the data of 1 Hz using the proposed algorithms (core i5 7200U 2.5 GHz).)

In this study, the proposed algorithm is used to predict the double difference observation of the obstructed satellite through the visible satellite. There are two cases in practice: First, for a satellite in the current epoch, the observation data of the reference and the rover receivers are all normal. The Radio Technical Commission for Maritime (RTCM, 10403.2) standard phase and phase corrections are used to calculate the RTK on the rover receiver, and the algorithm of prediction is not enabled. Second, if any observation data of the reference or the rover receiver is loss, the user will enable the proposed algorithm before RTK positioning to predict the DD observation between the reference and the rover receivers, and then based on the observation data of the reference or the rover receiver, recovering the "raw" observations missing from another receiver. In extreme cases, there is no raw data for both the reference receiver and the rover. The observations of one receiver can be set to 0 or replaced by historical observations, and the other receiver can be recovered based on the predicted DD observations. As long as the DD observation of the recovering the "raw" observations is consistent with the predicted DD observation, and then transferred to the user standard RTK solution module, the positioning result output based on the proposed algorithm can be performed.

In summary, the proposed algorithm only needs to add an observation predicting and recovery module in the user

terminal before RTK positioning, and does not need to change the current RTCM coding strategy and standard RTK positioning algorithm. The proposed algorithm is a good universal solution.

### 2.6. Static experiment and kinematic deformation experiment

While demonstrating the effectiveness of our algorithm, the solution without missing data was considered the "reliable value". Although the value cannot be factually known, a prediction, upon verification and experience, may be considered sufficiently reliable. There are three states in which a satellite receiver may exist: static, kinematic deformation, and kinematic navigation. Four Schemes were considered in our study.

**Scheme 1:** Coordinate sequence information for prediction algorithm.
**Scheme 2:** DD observation prediction algorithm and D-P algorithm.
**Scheme 3:** DD observation prediction algorithm only.
**Scheme 4:** Exclusions satellite with missing observations data without prediction.

We assume that the C04 satellite observation is interrupted. Then, according to the process described in the previous section, the C01 satellite is used to predict the DD observation of the C04 satellite for the duration of the interruption. Fig. 5 shows a simulation of the data interruption sequence at 1-min intervals, with total duration of 30 min and an enlargement of 5 min. The single-epoch positioning algorithm used in this study is not affected by this assumption when the receiver reacquires the signals. The positioning accuracy of Scheme 2 is evaluated under three states of the receiver and compared with the accuracies of Scheme 1. Scheme 3 is included to verify the improvement resulting from the introduction of the D-P algorithm in the deformation experiment, in which the receiver state changes frequently.

On August 27, 2016, a short baseline of approximately 30 m was placed on the roof of a building. A receiver was placed on a static platform to act as the reference station. The rover receiver was mounted on an experimental mobile platform used to simulate the deformation, as shown in Fig. 6 (Receiver UNICORECOMM-UR380 which produced by the company of UNICORECOMM in China, Antenna HG-GOYH7151 which produced by the company of HIGH GAIN in China) (Tu et al., 2017c). The static data were collected for a period of time, and then the deformation simulation was performed using the experimental platform. The simulation started in the 4280th epoch. Table 3 shows the process times. The RTK solution sequence in the E, N, and U directions without the absence of missing data is shown in Fig. 7. These values are collectively treated as the "reliable" position for comparison with Scheme 1, Scheme 2, and Scheme 3. In this study, owing to the limitations of our experimental equipment, there is no simulation in the vertical direction. Any creeping effect from the vertical direction is a result of the orientation of the experimental platform, which is not strictly horizontal during the horizontal simulation, as shown in Fig. 7. The trajectory of satellites in the elevation and azimuth domain is shown in Fig. 8.

Owing to transmission link disturbances, urban canyon, and device failure, GNSS receivers often lose observation. In our study, we assume that the urban canyon effect reduces the number of satellites. The C02 C03 and C05 satellites are obstructed and the C04 satellite makes intermittent observations.

## 3. Results and discussion

### 3.1. Static experiment

To verify the effectiveness the algorithm in the static observation phase, an example of a comparison chart for the three Schemes is given in Fig. 9. The duration shown is 35 min, half of the duration assigned for static observation, and only includes the interruption period.

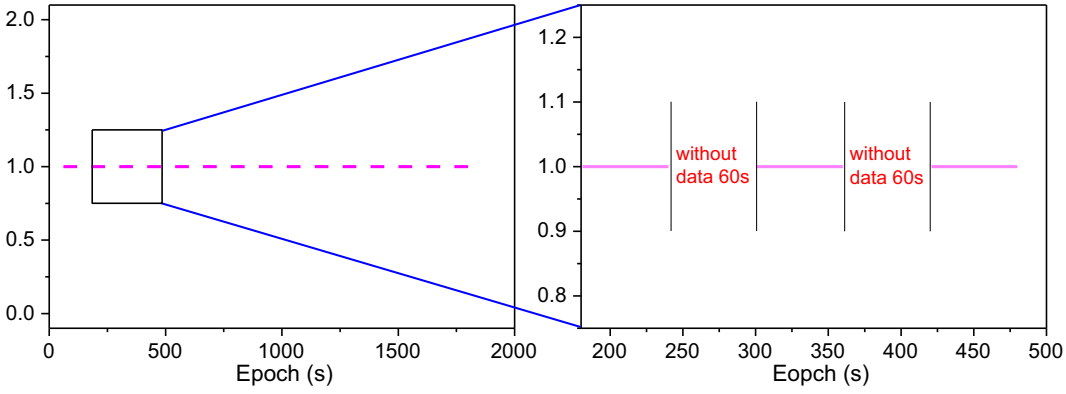


Fig. 5. Data interruption diagram.

Fig. 6. Experimental platform and rover antenna.

Table 3
The simulation of deformation process.

| Direction | Distance moved (cm) | Time (min) |
|---|---|---|
| North | 18 | 1 |
| Static | – | 3 |
| South | 39 | 7 |
| Static | – | 5 |
| North | 21 | 3 |
| Static | – | 3 |
| East | 18 | 3 |
| Static | – | 5 |
| West | 38 | 3 |
| Static | – | 3 |
| East | 20 | 2 |
| Static | – | 2 |
| Southwest | 17 | 5 |
| Static | – | 1 |
| Northeast | 39 | 3 |

It can be seen from Fig. 9 that the horizontal positioning accuracy of Scheme 2 is less than 0.5 mm, the vertical positioning accuracy less than 10 mm, and the residual in three directions from Scheme 1 is twice that obtained from Scheme 2. Scheme 4 and Scheme 2 are basically the same in the E direction, and the errors in the other two directions are lower than those in Scheme 2.

The statistical positioning accuracy data in Table 4 show that the horizontal accuracies of the two Schemes are better than their vertical accuracies. However, the RMS result from Scheme 1 is 3–4 times worse than that obtained from Scheme 2. The vertical RMS of the Scheme 1 is almost twice that of Scheme 2. Use of current epoch information ensures that the positioning accuracy of Scheme 2 is significantly higher than that of Scheme 1.

The sliding window for Scheme 1 is too small to accurately predict the multipath and noise parameters during observation (Dai et al., 2014; Ye et al., 2015; Qiu and Liu, 2016). By contrast, if the sliding window is too large, it becomes affected by state changes, and the resultant coordinate prediction are inaccurate. The window size for Scheme 1 is set at 30 s in static and 10 s in dynamic observations considering the resulting noise, receiver state, and 1-min interruption assumptions. These values are decided upon based on experience in order to ensure high accuracy in predictions. Nevertheless, the results are worse than those obtained from Scheme 2, because the window length for Scheme 2 is adaptively adjusted based on the receiver state.

It can be seen that for short-baseline real-time positioning, Scheme 2 can fully satisfy the accuracy requirement, and the impact of partial data loss can be resolved. Relative to Scheme 1, Scheme 2 has 75%, 70%, and 47% improvements in accuracy in the E, N, and U directions respectively.

### 3.2. Kinematic deformation experiment

Unlike in the static experiment, the state of the receiver during kinematic deformation is changing during the simulation. The sliding window for Scheme 2 can be adjusted in real time using the D-P algorithm. As described earlier, in this study, when the state of the receiver does not change, a window length of 30 s is used. If the receiver state changes, the process described in Section 2.4 is used. In order to verify the improvement resulting from the use of the

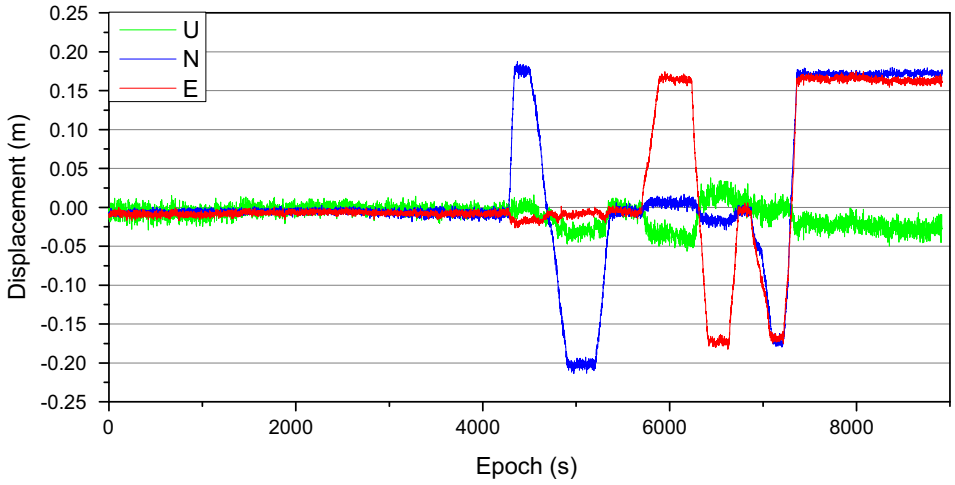


Fig. 7. E, N, U: the three directions of the experimental process sequence diagram. The figure shows displacement along these directions across the epochs.

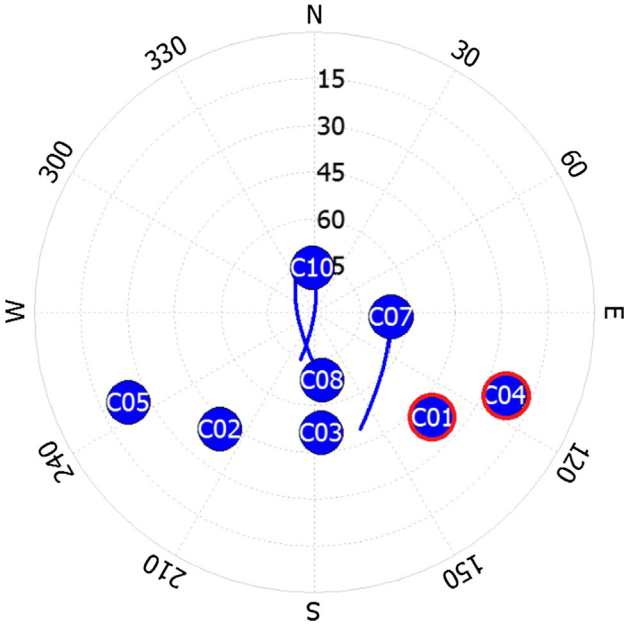


Fig. 8. Trajectory of satellites in the elevation and azimuth domain.

D-P algorithm in Scheme 2, we introduced Scheme 3, – in which the D-P algorithm is not used. The positioning accuracies of Scheme 4, Scheme 1, 2, and 3 are obtained by considering the solution without missing data to be the "reliable position", as shown in Fig. 10.

It can be seen in Fig. 10 that when the receiver state changes, the horizontal residual in Scheme 1 is greatly affected, with a maximum of 8 cm variation in the E direction and more than 10 cm in the N direction. Scheme 3 performs better than Scheme 1 in terms of horizontal positioning accuracy, but worse than Scheme 2. Vertical positioning accuracy exceeds 10 cm for Scheme 3.

The statistics in Table 5 show that the vertical RMS for Scheme 3 is 2.2 cm, but the values for Scheme 2 and Scheme 1 are <1.5 cm. The horizontal RMS for Scheme 2 is 0.2–0.4 cm, which is significantly better than the range

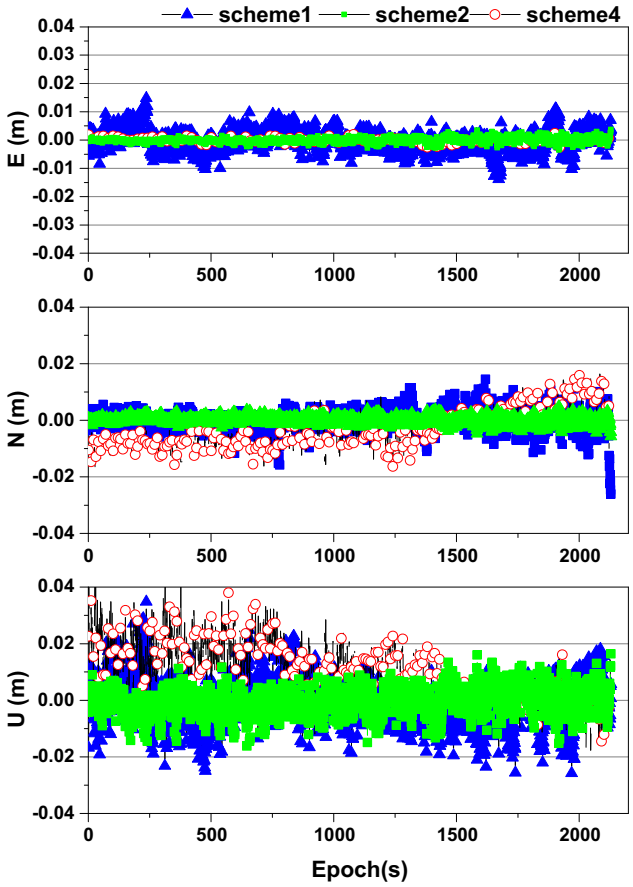


Fig. 9. Comparison between Scheme 1, 2 and 4 positioning results for the static experiment.

Table 4
RMS statistical results from the static experiment.

| Experimental program | Method | RMS (m) | | |
|---|---|---|---|---|
| | | E | N | U |
| Static | Scheme 1 | 0.0037 | 0.0038 | 0.0084 |
| | Scheme 2 | 0.0009 | 0.0012 | 0.0045 |
| | Scheme 4 | 0.0011 | 0.0077 | 0.0151 |

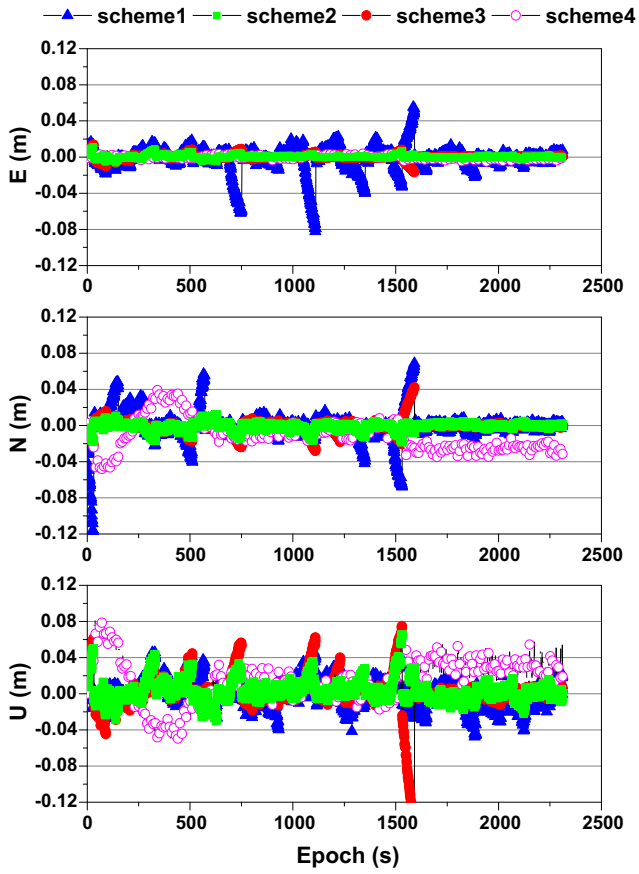


Fig. 10. Positioning results from the four Schemes for the deformation experiment.

for Scheme 1 (1.4–1.7 cm). Scheme 3 is affected by prediction biases during the interruption period in the dynamic simulation. The length of the sliding window in Scheme 3 cannot be adjusted in real time based on the state of the receiver. Particularly in the vertical direction, the noise from observation is significantly greater than in the horizontal direction, which causes the predictions to deviate from actual observations. However, the use of observations from other satellites at the current epoch and real-time adjustment of sliding window length ensure that the horizontal positioning precision provided by Scheme 2 is optimal. Because this study is limited by the experimental equipment, vertical positioning accuracy could not be improved significantly without a detailed simulation of deformation experiments. The creeping deformation is derived only from the experimental platform, which is not strictly horizontal during the horizontal simulation. Therefore, the vertical results are the same in the dynamic simulation as in the static experiment.

Table 5
RMS statistical results from the deformation experiment.

| Experimental program | Method | RMS: m | | |
|---|---|---|---|---|
| | | E | N | U |
| Deformation | Scheme 1 | 0.014 | 0.017 | 0.014 |
| | Scheme 2 | 0.002 | 0.004 | 0.011 |
| | Scheme 3 | 0.003 | 0.007 | 0.022 |
| | Scheme 4 | 0.003 | 0.021 | 0.029 |

From the deformation experiment we find that: 1. the positioning accuracy obtained is slightly lower than that obtained from the static phase, but it can still meet requirements for deformation monitoring. 2. The introduction of the D-P algorithm changes the length of the sliding window according to real-time receiver state changes, and thus improves prediction reliability. 3. Relative to Scheme 1, Scheme 2 results in 85%, 76%, and 27% improvement in prediction in the E, N, and U directions respectively.

### 3.3. Kinematic navigation experiment

To further verify the effectiveness of Scheme 2 in dynamic navigation, the rover receiver was mounted on the roof of a car, with the distance between the reference receiver and the rover receiver set at approximately 6.5 km. We chose the open environment for experiment. And the data loss statistics for two frequencies are 00.07% and 00.14% respectively. The results can be used as "reliable values" to compare with simulation experiments. Then, in the study, the navigation experiment solution is the simulation result. Data interrupted every minute for one minute, increasing the data loss rate to 50% for the simulation experiment. The car moving on the road was tracked for approximately 10 min. The equipment used was the same as that used for our static simulation experiment, and the sample rate was 1 Hz. It can be seen from Fig. 11 that there are nine satellites in the elevation and azimuth domain. We assume that because the satellites signals were obstructed, only signals from satellites C01, C04, C06, C09 and C12 can be received. The C04 satellite makes

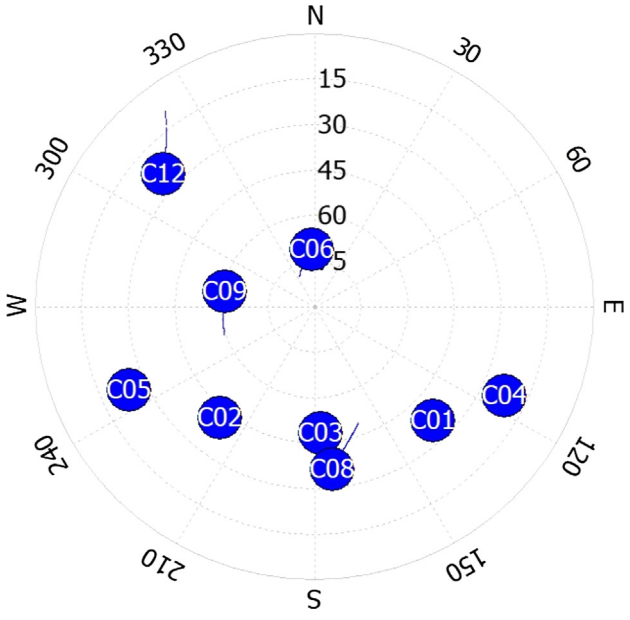


Fig. 11. Trajectory of satellites in the elevation and azimuth domain.

intermittent observations as shown in Fig. 5. As we have proved that use of a D-P algorithm improves the prediction accuracy, only Scheme 1, 2 and 4 were compared. The trajectory followed by the car is shown in Fig. 12. We enlarged the north-south direction. The resulting proportion of the trajectory does not reflect reality, but it can reflect the positioning results given by the two prediction algorithms. The trajectories predicted by the two Schemes are compared with the "reliable" trajectory. It can be seen from Fig. 12 that when the motion direction of the rover changes, the Scheme 1 results deviated from the actual trajectory, whereas Scheme 2 results coincided with the actual trajectory to a high degree as shown in Table 6. The positioning errors produced by Scheme 0, 1 and 2 were obtained by considering the solution without missing data to be the "reliable" result, as shown in Fig. 13. The difference between the errors of the two Schemes is too large to be depicted in the same coordinate system. It can be seen that the vertical prediction errors produced by Scheme 2 are worse when compared with the results from our static experiments, but significantly better than those produced by Scheme 1. The result of Scheme 1 is derived from the prediction of the coordinate sequence, which makes use of the historical coordinate information. When the receiver changes its movement direction, as shown in Fig. 12, the Scheme 1 is significantly deviated, which also contributes to the large error. The magnitude of the residual in the E direction is the smallest. This is because the configuration of the GEO satellites is such that they were distributed in the east–west direction in the BDS system (Zhang et al., 2015). It can be seen that Scheme 2 in the horizontal direction satisfied the requirement of 2 dm to meet the criteria of lane-level positioning. Especially in urban settings, a great deal of data loss occurs, so the improved results obtained from this algorithm are highly significant.

It can be seen from the above results, the accuracy indexes of Scheme 4 are larger than that of Scheme 2 in all three experiments. From Fig. 11(c), Scheme 4 seems to contain significant systematic errors in N and U directions, which dues to the less visible satellites in Scheme 4.

Table 6
RMS statistical results for kinematic navigation experiment.

| Experimental program | Method | RMS: m | | |
|---|---|---|---|---|
| | | E | N | U |
| Navigation | Scheme 1 | 52.460 | 3.356 | 1.820 |
| | Scheme 2 | 0.010 | 0.066 | 0.173 |
| | Scheme 4 | 0.042 | 0.264 | 0.555 |

### 3.4. Results for different baseline lengths

In order to verify the positioning results of the algorithm under different baseline lengths, the following experiments were added. The baselines with three lengths are 20 km, 50 km and 103 km. For a total of 1 h of data collection, the sampling rate is 1 Hz. The results of Scheme 2 are shown in Fig. 14 and Table 7. As the baseline becomes longer, the correlation of the atmospheric error is weakened, which affects the elimination of the DD errors (Takasu and Yasuda, 2010). From the results, the damping in the vertical direction is more obvious. This is because the vertical dilution of precision is larger than the horizontal dilution of precision, and the atmospheric error is projected mostly in the height component (Zhang et al., 2015).

The results of the static and kinematic experiments demonstrate that Scheme 2 achieves high-accuracy positioning. When valid satellite observations could not support normal RTK positioning, Scheme 2 produced higher positioning accuracy and was better to use than Scheme 1.

## 4. Conclusions

This study proposed an algorithm to predict DD observations of BDS GEO satellites. We introduced a

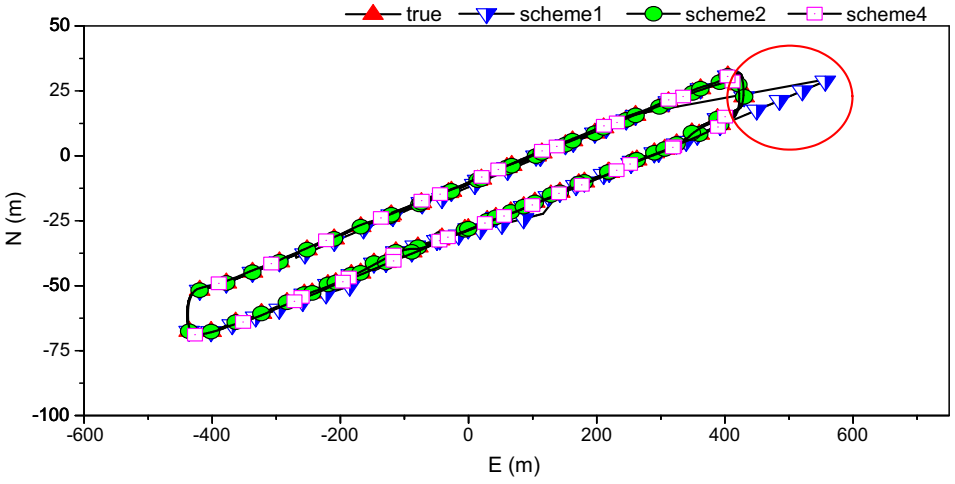


Fig. 12. Track graph comparison chart.

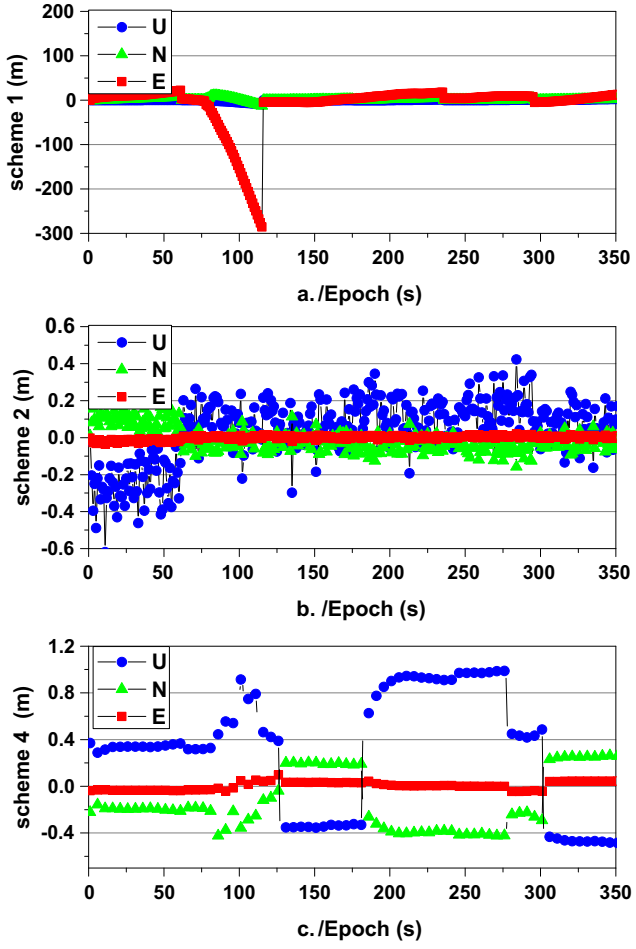


Fig. 13. Positioning results from the three Schemes for the navigation experiment.

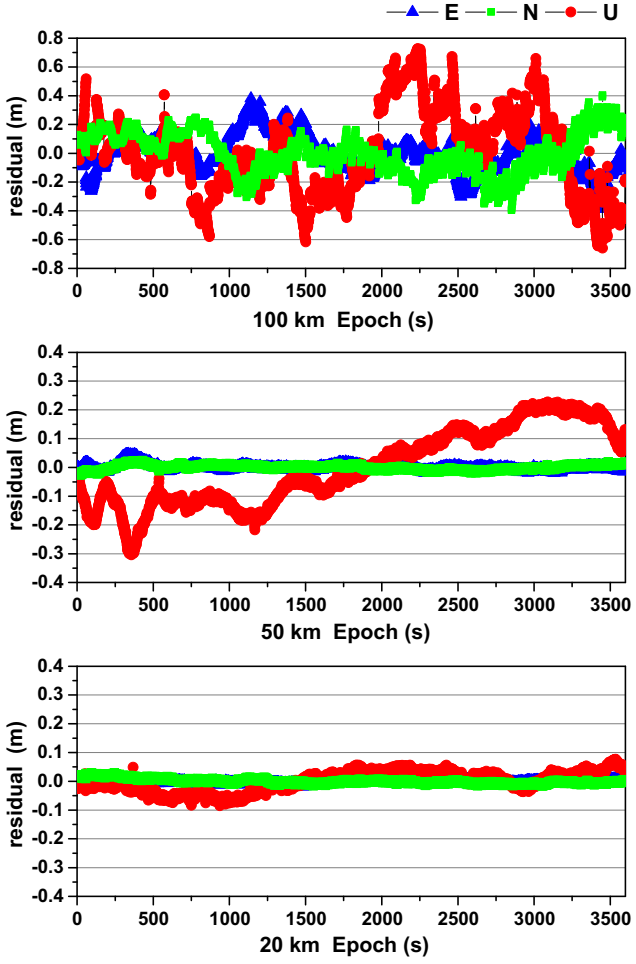


Fig. 14. Positioning results from the three different baseline lengths.

D-P algorithm to judge the state of the rover receiver to reduce the impact of predictive biases in the overall predictive algorithm. In the static experiment, our proposed algorithm produced an output in good agreement with the original sequence, and the RMS value was <5 mm. In the deformation experiment, the RMS value of the proposed algorithm was <2 cm, meeting the requirements for real-time deformation monitoring. The navigation experiment yielded a horizontal positioning accuracy of <10 cm and vertical positioning accuracy of <20 cm. Therefore, the proposed algorithm has high practical value in static, deformation, and navigation applications. In addition, as the baseline becomes longer, the accuracy is weakened. Owing to limitations in available experimental equipment, we could not conduct a simulation in the vertical direction. Furthermore, this study only considered the observations lost by GEO satellites. There is a significant correlation between the GEO satellites DD observation values adopted in the data processing of predicting. However, IGSO and MEO satellites are not fixed in the sky, and the correlation between the satellites is relatively weak. Further work is certainly required to disentangle the complexities of the correlation between satellites. This provides a good starting point for discussion and further research. It is difficult but necessary to introduce new prediction algorithms in particular, recent new algorithms in GNSS data processing, such as BP neural network (Huang et al., 2018) and deep learning to adapt to this difference. In future research, we will focus on the applicability of this algorithm to IGSO and MEO satellites.

Table 7
RMS statistical results for three different baseline lengths.

| Lengths | RMS: m | | |
|---|---|---|---|
| | E | N | U |
| 103 km | 0.132 | 0.143 | 0.292 |
| 50 km | 0.009 | 0.010 | 0.135 |
| 20 km | 0.007 | 0.009 | 0.036 |

## Acknowledgments

This work is supported by our research group. This research was partly supported by the National Natural Science Foundation of China (Grant Nos. 41731066, 41774025, 41504006 and 41674034), the program of

National Key Research and Development Plan of China (Grant No. 2016YFB0501804), the Program of the Grand Projects of the BeiDou-2 System (Grant No. GFZX0301040308), the National Natural Science Foundation of Shan Xi (Grant No. 2016JQ4011), the Chinese Academy of Sciences (CAS) programs of Pioneer Hundred Talents and the Frontier Science Research Project (Grant No. QYZDB-SSW-DQC028), and the Special Fund for Basic Scientific Research of Central Colleges (Grant Nos. 310826172006, 310826172202, 310826173101, Chang'an University). We would like to thank Editage [www.editage.cn] for English language editing.

## References

Comstock, S.J., 2006. Development of a Low-Latency, High Data Rate, Differential GPS Relative Positioning System for UAV Formation Flight Control Master's thesis. Air Force Institute of Technology.

Dai, W., Huang, D., Cai, C., 2014. Multipath mitigation via component analysis methods for GPS dynamic deformation monitoring. GPS Sol. 18 (3), 417–428. https://doi.org/10.1007/s10291-013-0341-9.

Douglas, D.H., Peucker, T.K., 2011. Algorithms for the reduction of the number of points required to represent a digitized line or its caricature. Can. Cartogr. 10 (2), 112–122. https://doi.org/10.3138/FM57-6770-U75U-7727.

He, L., Ge, M., Wang, J., Wickert, J., Schuh, H., 2013. Experimental study on the precise orbit determination of the BeiDou navigation satellite system. Sensors 13 (3), 2911–2928.

Huang, G.W., Zhang, Q., 2012. Real-time estimation of satellite clock offset using adaptively robust Kalman filter with classified adaptive factors. GPS Sol. https://doi.org/10.1007/s10291-012-0254-z.

Huang, G.W., Cui, B., Zhang, Q., et al., 2018. An improved predicted model for BDS ultra-rapid satellite clock offsets. Remote Sens. 10 (1), 60. https://doi.org/10.3390/rs10010060.

Jin, S., 2016. Preface: BeiDou navigation satellite system (BDS)/GNSS+: recent progress and new applications. Adv. Space Res. 59 (3). https://doi.org/10.3390/s17122761.

Lawrence, D.G., 1999. Reference Carrier Phase Prediction for Kinematic GPS. US Patent 5,903,236.

Leick, A., 2004. GPS Satellite Surveying, third ed. Wiley, Hoboken, pp. 172–177, ISBN: 978-0-471-05930-1.

Montenbruck, O., Schmid, R., Mercier, F., Steigenberger, P., Noll, C., Fatkulin, R., Kogure, S., Ganeshan, A.S., 2015. GNSS satellite geometry and attitude models. Adv. Space Res. 56 (6), 1015–1029. https://doi.org/10.1016/j.asr.2015.06.019.

Qiu, X., Liu, G., 2016. Influence analysis of BDS/GPS observation noise on ambiguity resolution. J. Navigat. Position. 4 (4), 69–76.

RTCM Standard 10403.2 Differential GNSS Services, Version 3 with Ammendment 2 (RTCM, Arlington 2013).

Shi, C., Zhao, Q., Hu, Z., Liu, J., 2013. Precise relative positioning using real tracking data from COMPASS GEO and IGSO satellites. GPS Sol. 17 (1), 103–119. https://doi.org/10.1007/s10291-012-0264-x.

Takasu, T., Yasuda, A., 2010. Kalman-filter-based integer ambiguity resolution strategy for long-baseline RTK with ionosphere and troposphere estimation. Proc. Int. Tech. Meet. Satell. Div. Instit. Navig. 7672 (6), 161–171.

Teunissen, P.J.G., De Jonge, P.J., Tiberius, C.C., 1997. The least-squares ambiguity decorrelation adjustment: its performance on short GPS baselines and short observation spans. J. Geod. 71, 589–602.

Teunissen, P.J.G., 2013. BLUE, BLUP and the Kalman filter: some new results. J. Geod. 87 (5), 461–473. https://doi.org/10.1007/s00190-013-0623-6.

Teunissen, P.J.G., Odolinski, R., Odijk, D., 2014. Instantaneous BeiDou + GPS RTK positioning with high cut-off elevation angles. J. Geod. 88 (4), 335–350. https://doi.org/10.1007/s00190-013-0686-4.

Tu, R., Zhang, R., Lu, C., Zhang, P., Liu, J., Lu, X., 2017a. A unified model for BDS wide area and local area augmentation positioning based on raw observations. Sensors 17 (3), 507. https://doi.org/10.3390/s17030507.

Tu, R., Lu, C., Zhang, P., Zhang, R., Liu, J., Lu, X., 2017b. The study of BDS RTK algorithm based on zero-combined observations and ionosphere constraints. Adv. Space Res. https://doi.org/10.1016/j.asr.2017.07.023.

Tu, R., Liu, J., Lu, C., Zhang, R., Zhang, P., Lu, X., 2017c. Cooperating the BDS, GPS, GLONASS and strong-motion observations for real-time deformation monitoring. Geophys. J. Int. 209 (3). https://doi.org/10.1093/gji/ggx099.

Wang, H., Ou, J., Yuan, Y., 2011. Strategy of data processing for GPS rover and reference receivers using different sampling rates. Geosci. Remote Sens. IEEE Trans. 49 (3), 1144–1149. https://doi.org/10.1109/TGRS.2010.2070509.

Wu, Z., Bian, S., Ji, B., Xiang, C., Jiang, D., 2016. Short baseline GPS multi-frequency single-epoch precise positioning: utilizing a new carrier phase combination method. GPS Sol. 20 (3), 373–384. https://doi.org/10.1007/s10291-015-0447-3.

Xu, G., Xu, Y., 2016. GPS: Theory, Algorithms and Applications. Springer Publishing Company, Incorporated.

Yang, Y.X., Li, J.L., Xu, J.Y., Tang, J., Guo, H.R., He, H.B., 2011. Contribution of the compass satellite navigation system to global PNT users. Sci. Bull. 56 (26), 2813. https://doi.org/10.1007/s11434-011-4627-4.

Ye, S., Chen, D., Liu, Y., Jiang, P., Tang, W., Xia, P., 2015. Carrier phase multipath mitigation for BeiDou navigation satellite system. GPS Sol. 19 (4), 545–557. https://doi.org/10.1007/s10291-014-0409-1.

Zhang, L., Lv, H., Wang, D., Hou, Y., Jie, W., 2015. Asynchronous RTK precise DGNSS positioning method for deriving a low-latency high-rate output. J. Geod. 89, 641–653. https://doi.org/10.1007/s00190-015-0803-7.